



Frequency tuning for broadband terahertz emission from two-color laser-induced air plasma

LINZHENG WANG,^{1,2}  ZHELIN ZHANG,^{1,2,3}  TIANHAO XIA,^{1,2} YANPING CHEN,^{1,2,*}  AND
ZHENGMING SHENG^{1,2,3,4,5} 

¹Key Laboratory for Laser and Plasma (Ministry of Education), School of Physics and Astronomy, Shanghai Jiaotong University, Shanghai, China

²Collaborative Innovation Centre of IFSA, Shanghai Jiaotong University, Shanghai, China

³Tsung-Dao Lee Institute, Shanghai, China

⁴Department of Physics, SUPA, University of Strathclyde, Glasgow, UK

⁵Cockcroft Institute, Sci-Tech Daresbury, Warrington, UK

*Corresponding author: yanping.chen@sjtu.edu.cn

Received 29 September 2021; revised 21 December 2021; accepted 21 December 2021; posted 22 December 2021;
published 28 January 2022

Effective manipulation of broadband terahertz emission, especially on spectrum tuning, is of great importance for many applications. We demonstrate a method to realize frequency tuning of terahertz emissions from two-color laser-induced air plasmas. The terahertz central frequency is switched from 0.56 to 0.82 THz by changing the polarization state of the fundamental wave with a quarter-wave plate. Based on numerical simulation, it is found that this frequency tuning is due to the birefringence effect induced by the fundamental wave on the second harmonic inside the filament, which leads to a discrepancy on the polarization chirality of the two-color laser components. Two-color lasers with opposite chirality will emit terahertz radiation with higher central frequency compared to two-color lasers with the same chirality at moderate laser intensity. © 2022 Optica Publishing Group

<https://doi.org/10.1364/JOSAB.444735>

1. INTRODUCTION

Terahertz radiation, which lies in the frequency range 0.3–30 THz, is of great importance for a wide range of applications in communication [1,2], imaging [3,4], biomedical science [5,6] and materials analysis [7,8]. Of particular interest for these applications, laser-induced air plasma is a prevalent way to generate terahertz emission due to its high field strength, broad spectrum, and high flexibility [9–13]. For example, effective manipulation of terahertz emission polarization [14,15], carrier envelope phase [16] as well as spectrum [12,17] have been realized, which greatly enriches its application scenarios.

In many applications, spectrum tuning for broadband terahertz radiation is critical. For example, in security applications, spectrum tuning could improve the accuracy of inspection for different substances [18]. In biochemistry, isomers of a biomacromolecule feature with different bio-signatures in a certain spectral region within the terahertz band [19]. Thus, fine control of the terahertz spectrum can considerably improve discrimination confidence. As for communication applications, matrix structures of terahertz absorbers always work at a few specific frequencies in order to expand its storage capability [20]. Through spectrum tuning, the accuracy of reading and writing of the matrix structures can be greatly improved.

For terahertz radiation from laser-induced air plasma, it is now well established that spectrum tuning of terahertz emitted

from laser-induced air plasma can be realized by either modulating the pump laser [21–23] or introducing an extra DC-bias [24,25]. Yamaguchi *et al.* demonstrated that the peak frequency of the terahertz radiation can be tuned by introducing different phase configurations to the pump with a spatial light modulator [21]. Wang *et al.* found that the terahertz spectrum can be controlled by tailoring the two-color laser beam with an iris, which have effects on the plasma distribution along the filament [22]. Massaoui *et al.* presented that the characteristics of the filament can be modulated by introducing a distortion in the laser beam wavefront, which led to the adjustment of the waveform as well as spectrum [23]. Furthermore, Wang *et al.* [24] and Zhang *et al.* [25] found that the central frequency of the terahertz radiation can be shifted by applying an external DC-bias in a two-color laser scheme.

In this paper, we experimentally demonstrate a method for frequency tuning between two central frequencies for terahertz emission from two-color laser-induced air plasma. The terahertz central frequency is tuned from 0.56 to 0.82 THz by changing the polarization state of the fundamental wave with a quarter-wave plate. The mechanism of such phenomenon is attributed by the birefringence effect induced by the fundamental wave inside the filament, which leads to a discrepancy on the polarization chirality of the two-color laser components. A two-color laser with opposite chirality will emit terahertz radiation with higher central frequency compared to a two-color laser with the

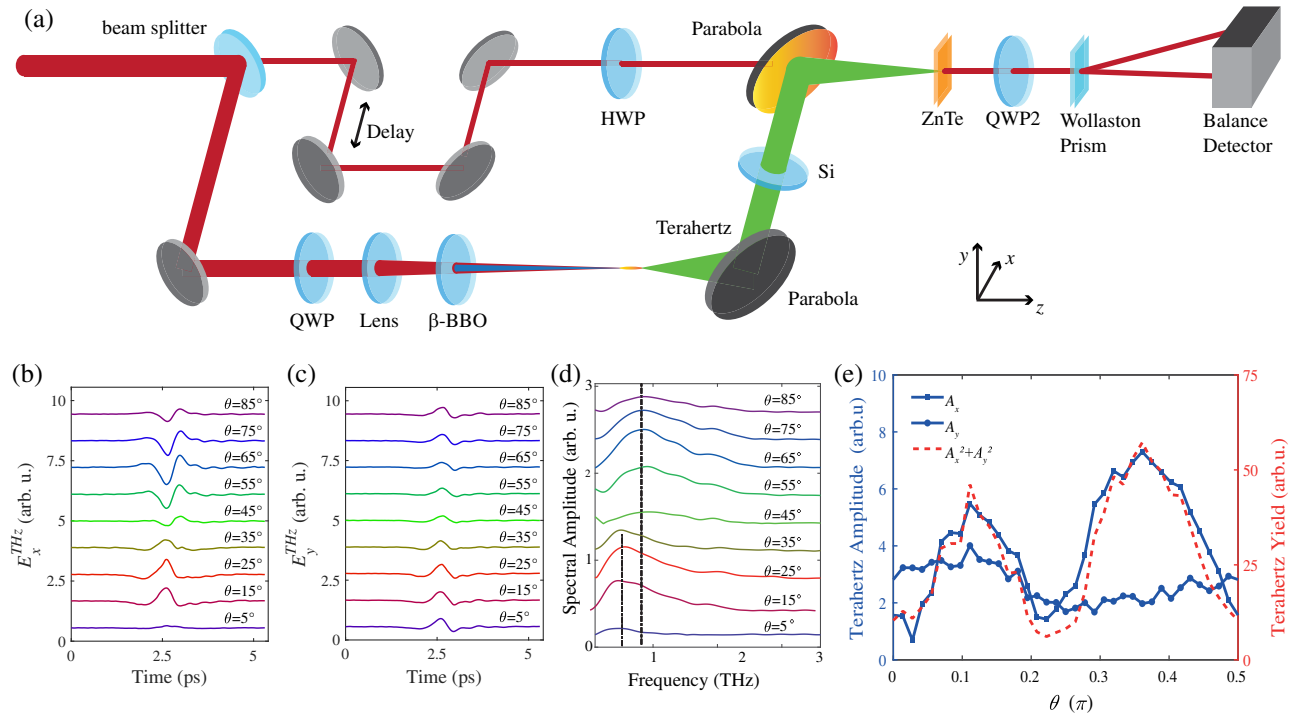


Fig. 1. Experimental setup and results. (a) Schematic of the experimental setup. (b) and (c) are the measured terahertz waveforms on the x -direction and the y -direction and (d) the terahertz spectra. (e) The peak-to-peak amplitudes of the terahertz waveforms and the total terahertz yield measured at different QWP angles. HWP, half-wave plate at 800 nm. QWP2, quarter-wave plate at 800 nm.

same chirality in the experiment. This work provides a simple way to realize terahertz frequency tuning.

2. EXPERIMENT AND RESULTS

An experimental setup is sketched in Fig. 1(a) for the generation and detection of terahertz pulses emitted from a laser filament excited by two-color laser pulses in air. A fundamental wave (FW) with 1.8 mJ pulse energy, 1 kHz repetition rate, and 35 fs pulse duration at 800 nm is intercepted by a β -barium borate (BBO) crystal of type-I phase matching, which leads to its second harmonic (SH) generation. The extraordinary axis of the BBO crystal is fixed along the y -direction in the experiment, which delivers an SH with y -oriented linear polarization. Initially, the FW is linearly polarized, and its orientation is parallel to the x -direction. The polarization of the FW can be changed by introducing a quarter-wave plate (QWP) at 800 nm to the FW beamline. The angle θ is defined as the angle between the fast axis of the QWP and the x -direction. The FW and its SH are focused into air by a lens of 50 cm focal length, forming a two-color laser filament with 12 mm length and $\sim 100 \mu\text{m}$ diameter. The terahertz radiation from this filament is collected by a pair of off-axis parabolic mirrors and then measured by the electro-optic sampling method with a 1-mm-thick ZnTe (110) crystal [26]. A silicon wafer is used to separate the terahertz radiation from the pump laser.

We measured the terahertz radiation from the two-color air plasmas on two orthogonal directions (E_x^{THz} and E_y^{THz}) by counterclockwise rotating the angle of the QWP θ , as shown in Figs. 1(b) and 1(c), respectively. The total terahertz yield

can be obtained through $A_x^2 + A_y^2$, where A_x and A_y are the peak-to-peak amplitudes of E_x^{THz} and E_y^{THz} , respectively. When θ changes from 0 to $\pi/4$, i.e., the FW polarization changes from linear to circular, the emitted terahertz yield increases first and then decreases to a minimum around $\theta = \pi/4$, as shown in Fig. 1(e). Then, we continue to counterclockwise rotate the angle of the QWP from $\theta = \pi/4$ (circularly polarized FW) to $\theta = \pi/2$ (linearly polarized FW) and the emitted terahertz yield increases first and decreases again. It is obvious that the terahertz radiation is quite sensitive to the FW polarization. Meanwhile, the evolution of terahertz spectrum as a function of the angle of the QWP θ is shown in Fig. 1(d). It is notable that its central frequency can be switched abruptly from ~ 0.56 THz ($\theta < \pi/4$) to ~ 0.82 THz ($\theta > \pi/4$), which is accompanied by a flip in the polarity of the terahertz electric field E_x^{THz} , as shown Fig. 1(b).

3. THE FW-INDUCED BIREFRINGENCE EFFECT ON THE POLARIZATION OF A TWO-COLOR LASER FIELD

In order to investigate the origin of the frequency switch effect, we first focus on the polarization evolution of the two-color laser components when rotating the angle of the QWP. The incident FW is linearly polarized at the x -direction when $\theta = 0$, so its electric field in the laboratory coordinate can be expressed as

$$\mathbf{E}_L(t)|_{xoy} = |E^\omega| \exp(i\omega t) \begin{bmatrix} 1 \\ 0 \end{bmatrix}, \quad (1)$$

where $|E^\omega|$ and ω are the amplitude and the angular frequency of the FW, respectively. When the FW successively pass through

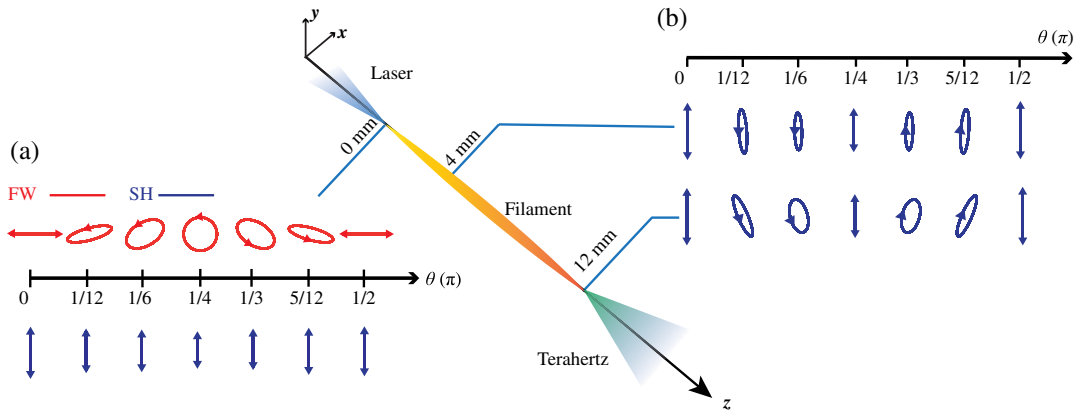


Fig. 2. (a) Calculated polarization of the FW and the SH as a function of θ at the beginning of the filament. (b) The polarization of the SH as a function of θ while propagating to $z = 4$ mm and $z = 12$ mm, respectively. The polarization chirality for the FW and the SH is displayed from the point of view of the receiver.

the QWP oriented at the angle of θ and a BBO crystal with extraordinary axis parallel to the y -direction, the two-color laser field can be derived as

$$\begin{aligned} \mathbf{E}_L(t)|_{xoy} = & |E^\omega| \exp(i\omega t) \begin{bmatrix} 1 - i \cos 2\theta & -i \sin 2\theta \\ -i \sin 2\theta & 1 + i \cos 2\theta \end{bmatrix} \begin{bmatrix} 1 \\ 0 \end{bmatrix} \\ & + R |E^\omega| \exp(i2\omega t) \begin{bmatrix} 0 \\ 1 \end{bmatrix}, \end{aligned} \quad (2)$$

where R is a coefficient considering both the SH conversion efficiency r and the change in the x -component of the FW when θ is varied, i.e.,

$$R = r \sqrt{\frac{1 + \cos^2 2\theta}{2}}. \quad (3)$$

In Eq. (2), the first term and the second term describe the electric fields of the FW and the SH, respectively. Thus, the polarization states of the FW and the SH at the beginning of the filament ($z = 0$) as a function of the QWP angle θ can be calculated, as shown in Fig. 2(a). When θ changes from 0 to $\pi/2$, the polarization ellipticity of the FW changes from 0 (linearly polarized FW) to 1 (circularly polarized FW) and eventually back to 0, while its polarization chirality remains left-handed. Meanwhile, the azimuth angle or the major axis of the FW polarization ellipse rotates by the same angle as the QWP angle θ . The SH remains linearly polarized for θ from 0 and $\pi/2$, with a modification in its amplitude according to Eq. (3).

When the two-color laser is focused into air, the ionized electrons in the air plasma acquire a drift velocity due to the asymmetric two-color laser field. These drifted electrons and ions will form a dipole that radiates a terahertz pulse [15]. This dipole can be derived as [15]

$$\mathbf{P} = \iint \mathbf{p} M(\mathbf{p})^* M(\mathbf{p}) d\mathbf{p}, \quad (4)$$

where \mathbf{p} is the momentums of the ionized electrons in a two-dimension matrix, and $M(\mathbf{p})$ is the probability amplitude of electrons in momentum space, which can be calculated using the strong field approximation (SFA) algorithm [27].

Based on Eqs. (2) and (4), the terahertz oscillating dipole as a function of the QWP angle θ can be calculated, as shown in Figs. 3(c)–3(g), for some typical cases. Initially $\theta = 0$, the orientation of the dipole is parallel to the y -direction. Later, the dipole swings around this initial orientation with increasing angle θ . The projections of the dipole amplitude on the x - and y -directions correspond to the terahertz amplitudes on the x - and y -direction s , respectively. In this way, the terahertz yield as a function of θ can be calculated, as shown in Fig. 3(a). The evolution of the simulated terahertz yield for $0 < \theta < \pi/4$ has the same tendency and the same peak value as that calculated for $\pi/4 < \theta < \pi/2$ [Fig. 3(a)], while the measured terahertz peak value for $0 < \theta < \pi/4$ is obviously lower than that for $\pi/4 < \theta < \pi/2$ [Fig. 1(e)]. This leads to the first discrepancy between the simulation and the observation.

Furthermore, according to Fig. 1(d), the central frequency of the emitted terahertz pulses measured as $0 < \theta < \pi/4$ is obviously lower than that measured as $\pi/4 < \theta < \pi/2$ in the experiment, which corresponds to a lower plasma frequency. The plasma frequency is calculated by [28] $\omega_p = \sqrt{4\pi n_e e^2/m}$, where n_e is the plasma density, and e and m are the charge and mass of an electron. A lower terahertz central frequency is attributed to a lower plasma density inside the filament. Based on a photocurrent model [29,30], however, the calculated ionization probabilities by two-color laser excitation with the QWP angle $\theta = \pi/6$ and $\theta = \pi/3$ reach the same value [Fig. 3(b)], i.e., the same plasma density. This leads to the second discrepancy between the simulation and the observation. Here, we choose $\theta = \pi/6$ and $\theta = \pi/3$ for comparison because these two cases are symmetric about the frequency switch point $\theta = \pi/4$.

In the simulation for Fig. 3(b), the plasma density is derived from the Ammosov-Delone-Krainov (ADK) tunneling model [29,31],

$$dn_e = w(t) N_0(t) dt, \quad (5)$$

where n_e is the plasma density, $w(t)$ the ADK ionization rate, and N_0 the residual molecule density. In our simulation, the laser intensity was taken as 5×10^{13} W/cm², which is around the clamping intensity for 800 nm laser in air [32]. Based on previous research [33], the first-order ionization of O₂ is about an

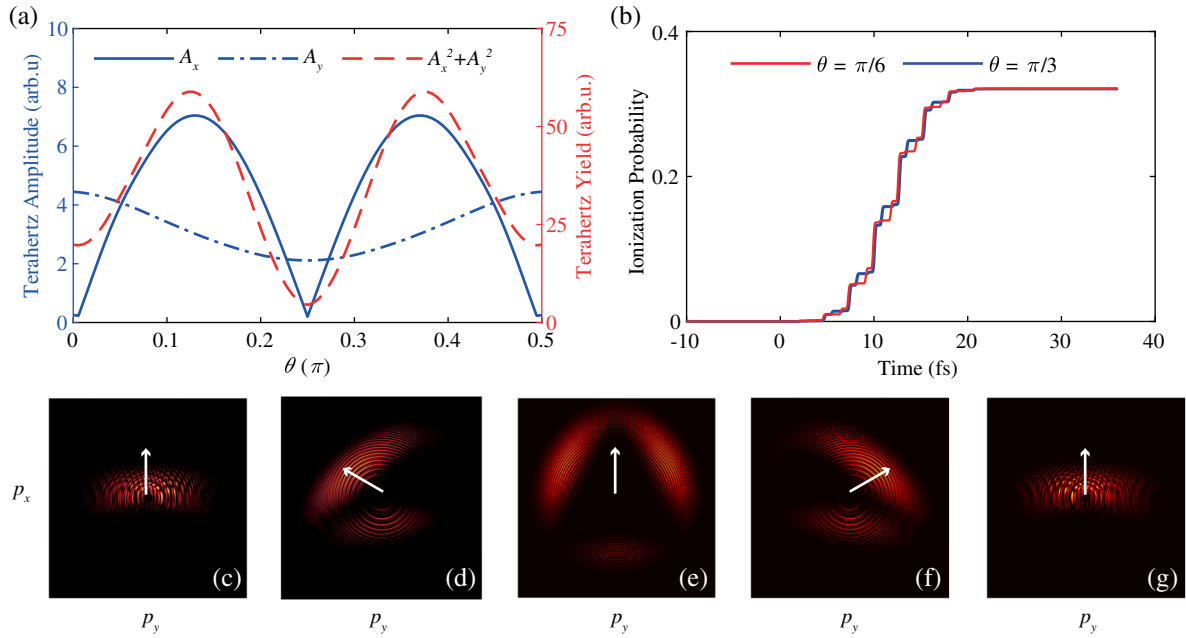


Fig. 3. Simulation results. The laser intensity was taken as 5×10^{13} W/cm² with 35 fs duration, which is close to the experimental parameters. The SHG efficiency is set to be 9% or $r = 0.3$ in Eq. (3). (a) Calculated terahertz amplitudes on the x -direction (solid line) and the y -direction (dot-dashed line), and the total terahertz yield (dashed line) at different QWP angles. (b) The time-dependent ionization probability with $\theta = \pi/6$ and $\pi/3$, respectively. (c)–(g) The corresponding electron distribution in momentum space with $\theta = 0, \pi/8, \pi/4, 3\pi/8$, and $\pi/2$. The dipole orientations are marked as white arrows.

order of magnitude larger than N_2 , which means the former is the dominant route of ionization for laser intensity in our experiment. Hence, only the first-order ionization of O_2 is taken into consideration with ionization potential energy $U_i = 12.06$ eV.

To understand the difference between experimental measurements and simulation results based upon the oscillating dipole model described above, one needs to carefully consider the coupling of the two-color laser components in plasma filaments, which leads to the polarization change of the SH component as described in the following. Actually, an intense FW can induce a strong change in the refractive index [34,35], and a filament would be anisotropic for a copropagating SH when the FW is not circularly polarized. This will introduce an additional birefringence-induced phase retardation to the copropagating SH as

$$\Delta\varphi^{2\omega} = \left(\frac{2\pi}{\lambda^{2\omega}} \right) n_2 \Delta I^\omega z, \quad (6)$$

where $n_2 = 7.4 \times 10^{-20}$ cm²/W is the nonlinear refractive index of air [34], $\lambda^{2\omega}$ is the wavelength of the SH, and z is the propagating length through the filament. ΔI^ω is the difference in FW intensities between the major and minor axes of its polarization ellipse, which can be indicated as

$$\Delta I^\omega = I^\omega \frac{1 - (\varepsilon^\omega)^2}{1 + (\varepsilon^\omega)^2}, \quad (7)$$

where I^ω and ε^ω are the intensity and the ellipticity of the FW, respectively.

Based on the above discussions, the polarization of the SH will be influenced by the FW-induced birefringence when these two laser components co-propagate along the filament. At

the position z of the filament, the two-color laser field can be expressed as

$$\begin{aligned} E_L(t, z)|_{xy} = & |E^\omega| \exp(i\omega t) \begin{bmatrix} 1 - i \cos 2\theta \\ -i \sin 2\theta \end{bmatrix} \\ & + R |E^\omega| \exp(i(2\omega t + \varphi + \Delta\varphi)) \\ & \times \left[\frac{\frac{1}{2} \sin 2\theta (1 - \exp(i\Delta\varphi^{2\omega}))}{\frac{1}{2}(1 + \exp(i\Delta\varphi^{2\omega})) + \frac{1}{2} \cos 2\theta (1 - \exp(i\Delta\varphi^{2\omega}))} \right], \end{aligned} \quad (8)$$

where φ is the initial relative phase between FW and SH, and $\Delta\varphi$ is the relative phase between FW and SH introduced by the linear dispersion of the plasma [35] during propagation inside the filament. In Eq. (8), the first term and the second term describe the electric fields of the FW and the SH after concerning the FW-induced birefringence during the co-propagation of these two laser components along a filament, respectively.

Based on Eq. (8), we can obtain the evolution of the SH polarization states as a function of the QWP angle θ after propagating for 4 mm ($z = 4$ mm) and 12 mm ($z = 12$ mm) inside the filament, as shown in Fig. 2(b). As is mentioned above, the filament is anisotropic for the SH due to FW-induced birefringence effect. Thus, the major axis of the FW polarization ellipse, rotating by the same angle as the QWP angle θ , decides the slow axis of the birefringent filament. The polarization of the SH keeps linear along the filament at $\theta = 0$ and $\pi/2$, as the SH polarization is perpendicular to the major axis of FW polarization ellipse. Meanwhile, the filament is isotropic when the FW is circularly polarized ($\theta = \pi/4$), i.e., no birefringence-induced phase is introduced for the SH, so the polarization of

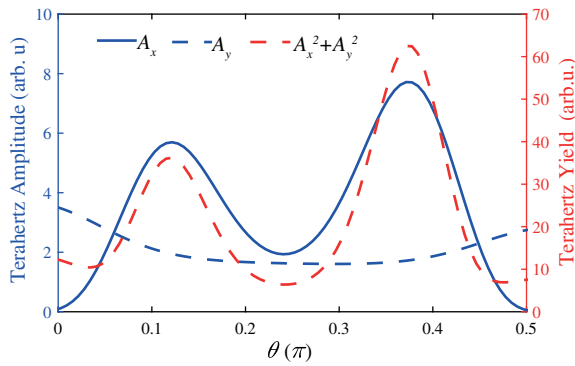


Fig. 4. Calculated terahertz amplitudes on the x -direction (solid line) and the y -direction (blue dashed line), and the total terahertz yield (red dashed line) at different QWP angles. In the simulation, the relative phase between the FW and the SH is $9\pi/16$, and the FW intensity is $5 \times 10^{13} \text{ W/cm}^2$. Other simulation parameters are the same as Fig. 3.

the SH stays linear along the filament too. In other cases, the polarization of the SH gradually becomes elliptical due to the FW-induced phase retardation to the SH. Furthermore, the chirality of the SH turns to left-handed for $0 < \theta < \pi/4$ and right-handed for $\pi/4 < \theta < \pi/2$ due to the orientation difference on the slow axis of the filament. For comparison again, if we focus on the SH polarization at $\theta = \pi/6$ and $\theta = \pi/3$, then the two typical cases locate symmetrically about the frequency switch point $\theta = \pi/4$. It is interesting to note that, after copropagating with the FW in the filament, the SH polarizations at these two cases feature the same polarization ellipticities but an opposite polarization chirality.

4. EFFECTS OF TWO-COLOR POLARIZATION CHIRALITY ON TERAHERTZ RADIATION

Using the two-color laser field expressed in Eq. (8), terahertz radiation from a dipole located at position z of the filament can be obtained. The total terahertz radiation from a long filament can be regarded as a superposition of terahertz radiation from each oscillating dipole located along the filament [15]. In this way, the terahertz peak-to-peak amplitudes on the x - and y -directions as well as the total terahertz yields can be calculated, as shown in Fig. 4. It is clear that the two peaks in the curve of the terahertz exhibit obvious differences after taking into account the FW induced birefringence effect, which is consistent with the experimental results [Fig. 1(e)]. Note that at $\theta = \pi/4$, the FW is circularly polarized, resulting in a lower ionization probability compared to the linearly polarized FW [33]. This leads to terahertz emission with a minimal yield at this QWP angle.

As discussed above, concerning the FW induced birefringence effect inside the filament, the polarization chirality of the SH is inverted around $\theta = \pi/4$ while the chirality of the FW remains left-handed. It has been well proven that the ionization process of atoms or molecules is closely related to the polarization [36] and the chirality of the laser field [37,38] as well as its intensity. Figures 5(a) and 5(b) depict the time-dependent ionization process as well as the electron current driving process at the FW intensity of $5 \times 10^{13} \text{ W/cm}^2$, which is close to our experimental condition (a laser filament in air), and a higher

FW intensity of $5 \times 10^{14} \text{ W/cm}^2$ (a gas jet in vacuum) [37,38], respectively. According to the photocurrent model [29,30], the drift current can be derived as

$$J(t) = \int_{t_0}^t e v_e(t, t') n_e(t') dt', \quad (9)$$

where $v_e(t, t')$ is the velocity of electrons born at $t = t'$ with the plasma density of $n_e(t')$, which can be derived by Eq. (5). In the simulation, the polarization and chirality of the two-color laser components utilized here is calculated at a filament position of $z = 4 \text{ mm}$ for the QWP angle of $\theta = \pi/6$ (FW left-handed and SH left-handed) and $\theta = \pi/3$ (FW left-handed and SH right-handed). Note that with higher laser intensity, the first-order ionization of N_2 with ionization potential energy $U_i = 15.506 \text{ eV}$ becomes the dominant route of ionization [33].

At the low laser intensity condition, as demonstrated in Fig. 5(a), only few cycles close to the center of the pulse duration can reach the threshold of ionization. It is obvious that the atoms are more easily ionized by the excitation of the two-color laser components with opposite chirality. This means that a slight difference caused by the superposition of the two-color laser field can lead to an apparent discrepancy on ionization probability at the end of the laser pulse, i.e., two-color laser components with opposite chirality provide higher ionization probability at this laser intensity. As the terahertz central frequency is close to the plasma frequency $\omega_p = \sqrt{4\pi n_e e^2 / m}$, a higher ionization probability promises a higher plasma density, and hence a terahertz radiation with a higher central frequency can be obtained from a filament excited by a two-color laser with opposite chirality. This result could qualitatively give an explanation for the experimental observation that the central frequency of the terahertz radiation obtained at $0 < \theta < \pi/4$ (FW left-handed and SH left-handed) is lower than that obtained at $\pi/4 < \theta < \pi/2$ (FW left-handed and SH right-handed).

As the laser intensity boosts high enough, the ionization probability will get saturated soon regardless of the chirality of the SH, as shown in Fig. 5(b). This means that the frequency switch phenomenon will not happen at such laser intensity. Moreover, Fig. 5(b) shows that the ionized electrons are more efficiently driven by a two-color laser field with the same chirality. As the terahertz radiation is proportional to the derivative of the residual drift current [29], terahertz radiation with higher power will be obtained from plasmas excited by a two-color laser with the same chirality. This phenomenon has been demonstrated experimentally with circularly polarized two-color laser-induced plasma [37]. On the contrary, the laser field of the circularly polarized two-color laser components with opposite chirality is symmetric. In this case, ionized electrons will not form a residual current, resulting in negligible terahertz emission [38]. Consequently, at low laser intensity, as in our experiment, two-color lasers with opposite chirality will emit terahertz radiation with a higher central frequency compared to two-color lasers with the same chirality. This leads to a frequency switch between 0.56 THz and 0.82 THz in the experiment. However, our simulation shows that this phenomenon disappears when the laser intensity is increased by one order of magnitude.

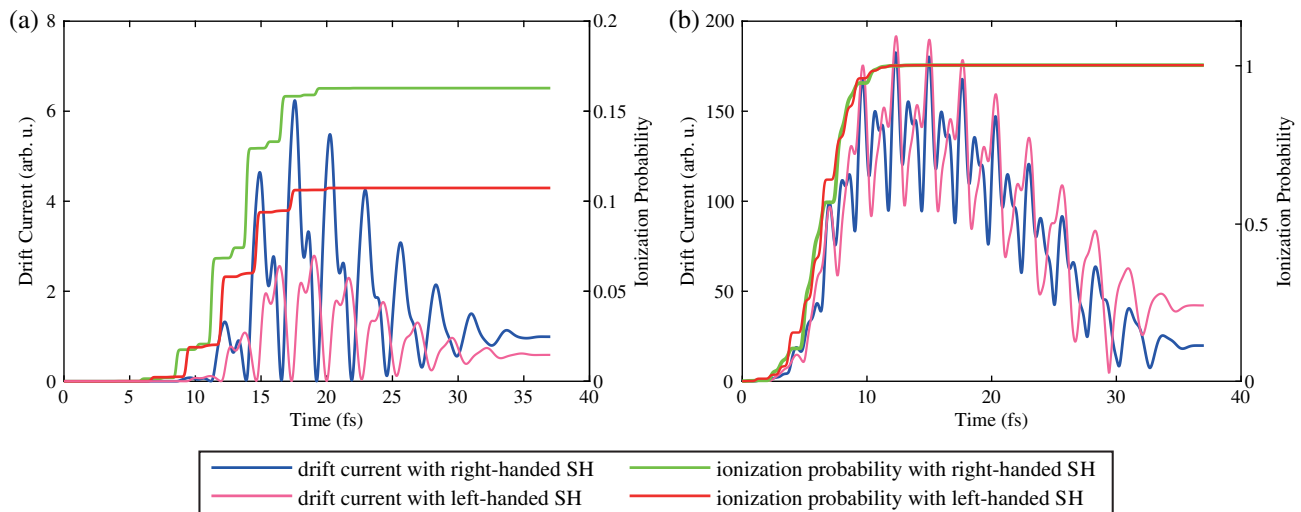


Fig. 5. Simulation results. The time-dependent ionization probability (red lines for left-handed SH and green lines for right-handed SH) and net drift current (pink lines for left-handed SH and blue lines for right-handed SH) with (a) the FW intensity 5×10^{13} W/cm² and (b) 5×10^{14} W/cm². The polarization chirality of the FW is left-handed, and the other simulation parameters are the same as Fig. 3.

5. CONCLUSIONS

In conclusion, we have experimentally demonstrated a method of central frequency switch for terahertz emission from two-color laser-induced air plasma. The central frequency of the broadband terahertz can be switched between 0.56 and 0.82 THz by changing the FW polarization with a QWP. Based on the theoretical analysis and numerical simulation, this frequency switch phenomenon is attributed to the FW-induced birefringence effect inside the filament, which modifies the polarization state of the co-propagating SH. Around the QWP angle for the frequency switch, the chirality of the SH is switched while the chirality of the FW remains left-handed. The chirality discrepancy would impact the ionization process as well as the following drift process of the electrons, which leads to the terahertz frequency switch as well as to the modulation on terahertz intensity. Our findings provide a simple method to realize frequency switch for broadband terahertz emission, which has potential applications in many research fields.

Funding. National Natural Science Foundation of China (11721091, 11774228, 11991073, 12074250); Science and Technology Commission of Shanghai Municipality (16DZ2260200).

Disclosures. The authors declare no conflicts of interest.

Data Availability. The data that support the plots in this paper and other findings of this study are available from the corresponding author upon reasonable request.

REFERENCES

1. T. Harter, C. Füllner, J. N. Kemal, S. Ummethala, J. L. Steinmann, M. Brosi, J. L. Hesler, E. Bründermann, A.-S. Müller, W. Freude, S. Randel, and C. Koos, "Generalized Kramers–Kronig receiver for coherent terahertz communications," *Nat. Photonics* **14**, 601–606 (2020).
2. J. Ma, N. J. Karl, S. Bretin, G. Ducournau, and D. M. Mittleman, "Frequency-division multiplexer and demultiplexer for terahertz wireless links," *Nat. Commun.* **8**, 729 (2017).
3. M. Li, X. Lv, J. Mou, D. Guo, H. Qiao, Z. Ma, and H. Hao, "340 GHz lens-coupled 4×4 GaAs detector array for terahertz imaging applications," *Electron. Lett.* **54**, 1180–1182 (2018).
4. Z. Yang, D. Tang, J. Hu, M. Tang, M. Zhang, H.-L. Cui, L. Wang, C. Chang, C. Fan, J. Li, and H. Wang, "Near-field nanoscopic terahertz imaging of single proteins," *Small* **17**, 2005814 (2021).
5. B. Breitenstein, M. Scheller, M. K. Shakfa, T. Kinder, T. Müller-Wirts, M. Koch, and D. Selmar, "Introducing terahertz technology into plant biology: a novel method to monitor changes in leaf water status," *J. Appl. Bot. Food Qual.* **84**, 158–161 (2011).
6. K. Johnson, "Terahertz vibrational properties of water nanoclusters relevant to biology," *J. Biol. Phys.* **38**, 85–95 (2012).
7. S. Kar, V. L. Nguyen, D. R. Mohapatra, Y. H. Lee, and A. K. Sood, "Ultrafast spectral photoresponse of bilayer graphene: Optical pump-terahertz probe spectroscopy," *ACS Nano* **12**, 1785–1792 (2018).
8. W. Lu, J. Ling, F. Xiu, and D. Sun, "Terahertz probe of photoexcited carrier dynamics in the Dirac semimetal Cd₃As₂," *Phys. Rev. B* **98**, 104310 (2018).
9. D. J. Cook and R. M. Hochstrasser, "Intense terahertz pulses by four-wave rectification in air," *Opt. Lett.* **25**, 1210–1212 (2000).
10. M. Kress, T. Löffler, S. Eden, M. Thomson, and H. G. Roskos, "Terahertz-pulse generation by photoionization of air with laser pulses composed of both fundamental and second-harmonic waves," *Opt. Lett.* **29**, 1120–1122 (2004).
11. J.-M. Manceau, A. Averchi, F. Bonaretti, D. Faccio, P. Di Trapani, A. Couairon, and S. Tzortzakis, "Terahertz pulse emission optimization from tailored femtosecond laser pulse filamentation in air," *Opt. Lett.* **34**, 2165–2167 (2009).
12. M. C. Hoffmann and J. A. Fülöp, "Intense ultrashort terahertz pulses: generation and applications," *J. Phys. D* **44**, 083001 (2011).
13. V. A. Andreeva, O. G. Kosareva, N. A. Panov, D. E. Shipilo, P. M. Solyankin, M. N. Esaulkov, P. G. de A. Martínez, A. P. Shkurinov, V. A. Makarov, L. Bergé, and S. L. Chin, "Ultrabroad terahertz spectrum generation from an air-based filament plasma," *Phys. Rev. Lett.* **116**, 063902 (2016).
14. Q. Song, X. Yuan, S. Hu, J. Huang, H. Zhong, Q. Lin, H. Wang, X. Lu, M. Zheng, Y. Cai, X. Zeng, and S. Xu, "Enhance terahertz radiation and its polarization-control with two parallel filaments pumped by two-color femtosecond laser fields," *Opt. Express* **29**, 22659–22666 (2021).
15. Z. Zhang, Y. Chen, S. Cui, F. He, M. Chen, Z. Zhang, J. Yu, L. Chen, Z. Sheng, and J. Zhang, "Manipulation of polarizations for broadband terahertz waves emitted from laser plasma filaments," *Nat. Photonics* **12**, 554–559 (2018).

16. Y. Kawada, T. Yasuda, and H. Takahashi, "Carrier envelope phase shifter for broadband terahertz pulses," *Opt. Lett.* **41**, 986–989 (2016).
17. Z. Zhang, Y. Chen, L. Yang, X. Yuan, F. Liu, M. Chen, J. Xu, Z. Sheng, and J. Zhang, "Dual-frequency terahertz emission from splitting filaments induced by lens tilting in air," *Appl. Phys. Lett.* **105**, 101110 (2014).
18. T. Yasuda, Y. Kawada, H. Toyoda, A. Nakanishi, K. Akiyama, and H. Takahashi, "Fast frequency-resolved terahertz imaging," *Rev. Sci. Instrum.* **82**, 034708 (2011).
19. D. L. Woolard, Y. Luo, B. L. Gelmont, T. Globus, and J. O. Jensen, "A bio-molecular inspired electronic architecture: Bio-based device concepts for enhanced sensing," *Proc. SPIE* **5790**, 180–194 (2005).
20. S. A. Kuznetsov, A. G. Paulish, A. V. Gelfand, P. A. Lazorskiy, and V. N. Fedorinin, "Matrix structure of metamaterial absorbers for multispectral terahertz imaging," *Prog. Electromagn. Res.* **122**, 93–103 (2012).
21. M. Yamaguchi and J. Das, "Terahertz wave generation in nitrogen gas using shaped optical pulses," *J. Opt. Soc. Am. B* **26**, A90–A94 (2009).
22. W. Sheng, F. Tang, Z. Zhang, Y. Chen, X.-Y. Peng, and Z.-M. Sheng, "Spectral control of terahertz radiation from inhomogeneous plasma filaments by tailoring two-color laser beams," *Opt. Express* **29**, 8676–8684 (2021).
23. M. Massaouti, J.-M. Manceau, A. Selimis, and S. Tzortzakis, "An intense tunable femtosecond gas-plasma THz source: Application in spectroscopic studies of polycyclic aromatic hydrocarbons," *J. Mol. Struct.* **1006**, 28–33 (2011).
24. T. Wang, C. Marceau, Y. Chen, S. Yuan, F. Théberge, M. Châteauneuf, J. Dubois, and S. L. Chin, "Terahertz emission from a dc-biased two-color femtosecond laser-induced filament in air," *Appl. Phys. Lett.* **96**, 211113 (2010).
25. Z. Zhang, Y. Chen, Z. Zhang, T. Xia, J. Zhang, and Z. Sheng, "Frequency blue shift of terahertz radiation from femtosecond laser induced air plasmas," *Appl. Phys. B* **127**, 11 (2021).
26. S. P. Kovalev and G. Kh. Kitaeva, "Terahertz electro-optical detection: optical phase or energy measurements," *J. Opt. Soc. Am. B* **30**, 2650–2656 (2013).
27. S. Cui and F. He, "Time-resolved ionization process of hydrogen atoms in strong laser fields," *Phys. Rev. A* **88**, 063412 (2013).
28. B. S. Mendoza and W. L. Mochán, "Ab initio theory of the Drude plasma frequency," *J. Opt. Soc. Am. B* **38**, 1918–1926 (2021).
29. K. Y. Kim, J. H. Glowina, A. J. Taylor, and G. Rodriguez, "Terahertz emission from ultrafast ionizing air in symmetry-broken laser fields," *Opt. Express* **15**, 4577–4584 (2007).
30. W.-M. Wang, Z.-M. Sheng, H.-C. Wu, M. Chen, C. Li, J. Zhang, and K. Mima, "Strong terahertz pulse generation by chirped laser pulses in tenuous gases," *Opt. Express* **16**, 16999–17006 (2008).
31. M. V. Ammosov, N. B. Delone, and V. P. Krainov, "Tunnel ionization of complex atoms and atomic ions in an alternating electromagnetic field," *Proc. SPIE* **0664**, 1191–1194 (1986).
32. J.-F. Daigle, A. Jaroń-Becker, S. Hosseini, T.-J. Wang, Y. Kamali, G. Roy, A. Becker, and S. L. Chin, "Intensity clamping measurement of laser filaments in air at 400 and 800 nm," *Phys. Rev. A* **82**, 023405 (2010).
33. C. Guo, M. Li, J. P. Nibarger, and G. N. Gibson, "Single and double ionization of diatomic molecules in strong laser fields," *Phys. Rev. A* **58**, R4271–R4274 (1998).
34. Y. S. You, T. I. Oh, and K.-Y. Kim, "Mechanism of elliptically polarized terahertz generation in two-color laser filamentation," *Opt. Lett.* **38**, 1034–1036 (2013).
35. O. Kosareva, N. Panov, V. Makarov, I. Perezhogin, C. Marceau, Y. Chen, S. Yuan, T. Wang, H. Zeng, A. Savel'ev, and S. L. Chin, "Polarization rotation due to femtosecond filamentation in an atomic gas," *Opt. Lett.* **35**, 2904–2906 (2010).
36. J. McKenna, M. Suresh, B. Srigengan, I. D. Williams, W. A. Bryan, E. M. L. English, S. L. Stebbings, W. R. Newell, I. C. E. Turcu, J. M. Smith, E. J. Divall, C. J. Hooker, A. J. Langley, and J. L. Collier, "Ultrafast ionization study of N₂ in intense linearly and circularly polarized laser fields," *Phys. Rev. A* **73**, 043401 (2006).
37. C. Meng, W. Chen, X. Wang, Z. Lü, Y. Huang, J. Liu, D. Zhang, Z. Zhao, and J. Yuan, "Enhancement of terahertz radiation by using circularly polarized two-color laser fields," *Appl. Phys. Lett.* **109**, 131105 (2016).
38. C. Tailliez, A. Stathopoulos, S. Skupin, D. Buožius, I. Babushkin, V. Vaičaitis, and L. Bergé, "Terahertz pulse generation by two-color laser fields with circular polarization," *New J. Phys.* **22**, 103038 (2020).